atmosphere

MDPI

Article

Investigation of the Pre- and Co-Seismic Ionospheric Effects from the 6 February 2023 M7.8 Turkey Earthquake by a Doppler Ionosonde

Nazyf Salikhov [1], Alexander Shepetov [1,2,*], Galina Pak [1], Serik Nurakynov [1], Azamat Kaldybayev [1,3], Vladimir Ryabov [2] and Valery Zhukov [2]

[1] Institute of Ionosphere, Almaty 050020, Kazakhstan; snurakynov@ionos.kz (S.N.)
[2] P. N. Lebedev Physical Institute of the Russian Academy of Sciences, Moscow 119991, Russia
[3] Institute of Experimental and Theoretical Physics, Al-Farabi Kazakh National University, Almaty 050040, Kazakhstan
* Correspondence: ashep@tien-shan.org

Abstract: During the catastrophic M7.8 earthquake in Turkey on 6 February 2023, anomalous effects were revealed in the ionosphere associated with various propagation mechanisms of seismogenic disturbance from the lithosphere up to the height of the ionosphere. Seventeen minutes after the main shock, a co-seismic disturbance was detected by a Doppler ionosonde on an inclined, 3010 km long, two-hop radio path "Kuwait—Institute of Ionosphere (Almaty)". An appearance of acoustic waves at the height of 232 km in the ionosphere was fixed 568 s after arrival of the surface Rayleigh wave to the sub-ionospheric point, and such a delay agrees with the calculated propagation time of a vertically moving acoustic wave. The disturbance lasted 160 s, and its double amplitude was above 2 Hz, which noticeably exceeds the background fluctuation of Doppler frequency. The best coincidence between the waveforms of the Doppler signal and of the surface seismic wave was observed over the duration of the two leading periods, with correlation coefficients of 0.86 and 0.79, correspondingly. Pre-seismic effects in the ionosphere were revealed 8 days before the main shock both in the variations of the Doppler frequency and of the critical frequency $f0F2$. The probable origination mechanism of the pre-seismic ionospheric disturbances above the region of the earthquake preparation determined by the Dobrovolsky radius may be considered in accordance with the concept of lithospheric–atmospheric–ionospheric coupling.

Keywords: Turkey earthquake; doppler frequency shift; ionosphere; rayleigh wave; acoustic wave; lithospheric–atmospheric–ionospheric coupling

Citation: Salikhov, N.; Shepetov, A.; Pak, G.; Nurakynov, S.; Kaldybayev, A.; Ryabov, V.; Zhukov, V. Investigation of the Pre- and Co-Seismic Ionospheric Effects from the 6 February 2023 M7.8 Turkey Earthquake by a Doppler Ionosonde. *Atmosphere* **2023**, *14*, 1483. https://doi.org/10.3390/atmos14101483

Academic Editors: Rui Yan, Michel Parrot, Zeren Zhima and Dedalo Marchetti

Received: 25 July 2023
Revised: 20 September 2023
Accepted: 21 September 2023
Published: 25 September 2023

1. Introduction

Large earthquakes, especially those that occur in the vicinity of cities and other considerable settlements, are accompanied by significant economic and social losses, casualties and injuries among population, and damage of urban infrastructure. Such were the consequences of the two catastrophic earthquakes that happened on 6 February 2023 in Turkey, in the region of the East Anatolian Fault and at the intersection of the three tectonic plates: Anatolian, Arabian, and African. The epicenters of both earthquakes were separated by a distance of ∼95 km and their sources were located at a depth of about 10 km. The first shock, with a magnitude $M_w = 7.8$ and geographical coordinates of the epicenter being N37.23° E37.02°, occurred at 01:17:34 UTC; the second $M_w = 7.3$ earthquake followed at 10:24 UTC; then, a series of strong aftershocks followed, lasting several days [1]. The effects that arose in the ionosphere both before and during the time of this catastrophic event are discussed in the present article.

The possible connection between the pressure waves from displacement of the earth's surface and the disturbances in the atmosphere and ionosphere was supposed for the first

time by K. Davis and D. Baker [2] on the basis of their Doppler observation of the ionosphere made by the method of Y. M. Watts and K. Davies [3], around the time of the Alaskan earthquake on 28 March 1968. This was also investigated by R. S. Leonard and R. A. Barns, who used the ionogram method [4]. In a prior review [5], most early observations reported on the disturbances in the upper atmosphere related with infrasonic sources, both of natural and artificial origin. During the next half-century and later, significant development proceeded in the investigation of the anomalous effects that arise in the ionosphere from the propagation of acoustic waves generated by surface seismic waves [6–8]. As a rule, disturbances from penetration into the ionosphere of the acoustic waves revealed 8–9 min later indicate an earthquake.

In the study of the possibility for acoustic waves to transmit the energy from the Earth into the upper atmosphere layers, considerable progress was achieved due to development of the method of Doppler radio sounding of the ionosphere. Thus, with an example of twelve M6.8–8.3 earthquakes, it was shown in [6] that even a tiny, below-millimeter displacement of the ground observed by propagation of a Rayleigh wave over the earth's surface may lead to vertical oscillation of about several tens of meters of ionosphere height and the resulting amplitude of the Doppler shift signal may be about (0.3–1.1) Hz. High effectiveness of the Doppler method for revealing the influence of acoustic waves onto the ionosphere was demonstrated even for the weak earthquakes [9–11] or for far-away earthquakes with a large epicenter distance [12,13].

In studies of the 1980–1990s, the acoustic mechanism of the generation of ionospheric disturbances was convincingly confirmed by data obtained at industrial and underground nuclear explosions. Disturbances in the ionosphere were distinctly revealed by the passage of acoustic waves from the explosion [14–16]. The physical nature of the influence of powerful explosions on the environment is similar to that of natural phenomena such as an earthquake.

At the same time, in the investigation of seismo-ionospheric signatures, certain difficulties were met, which were stipulated by sensitivity of the ionosphere to a variety of external influences, such as a high level of solar activity, geomagnetic storms, volcanic explosions, dust storms, tsunamis, etc. [17–23].

Taking into account the catastrophic consequences of large earthquakes, one of the most pressing problems of modern geophysics is revealing such ionospheric anomalies prior to an earthquake, which could be considered as a precursor of a seismic event. In the last decades, in a majority of works, the data from the satellites of the Global Navigation Satellite System (GNSS) were used for investigation of total electron concentration (TEC) before earthquakes. During that time, a lot of evidence was accumulated on the anomalous signals in the ionosphere preceding earthquakes, which were registered on magnetically quiet days and in the absence of any other disturbing events. In [24–27], short reviews are given of the seismogenic phenomena detected in the ionosphere by ground-based and satellite methods, which can be interpreted as possible precursors of an earthquake. For example, after exclusion of the days with a high level of solar activity and strong geomagnetic storms, noticeable anomalies in TEC variation were found 11–16 days before the M_s6.4 Yangbi and M_s7.4 Maduo earthquakes on 21 May 2021 [28]. With the help of the geostationary GNSS system Baidou, an unusual phenomenon in TEC variation was detected, which appeared during sunset hours $\sim$7 days before the M6.1 Dali and M7.3 Qinghai earthquakes [29]. In [30], an amplification of ionospheric TEC was reported immediately before the 2011 M_w9.0 earthquake in Tohoku-Oki. According to the opinion of the authors in [31], similar anomalies took place before all $M \geq 8.5$ earthquakes of the current century, which provides evidence for the seismogenic origin of such effects. In [32], unusual fluctuations in the ionosphere were reported, which were detected both by a Doppler sounding system, the net of ground-based GPS receivers, and an ionosonde before the two M7.0 earthquakes on 26 December 2006 near Pingtung, Taiwan.

Even before application of the satellite-based methods, such as GNSS, some anomalies associated with earthquakes were observed on the ground by receiving Very Low and Ultra-

Low Frequency (VLF/ULF) radio signals. Thus, noticeable precursory effects were revealed in a record of VLF subionospheric signals in the time of the large M_w6.8 earthquake in Kobe (Japan) on 17 January 1995 [33]. The perturbations caused by seismo-ionospheric coupling processes were detected in the propagation of the sub-ionospheric VLF signals prior to and in the time of the *M*7.3 Nepal earthquake on 12 May 2021. It was found that 3–4 days before the earthquake, the amplitude of the 22.2 kHz VLF signal from the Japan JJI transmitter was perceptibly diminishing at sunrise and sunset times [34]. Based on an analysis of the data on sub-ionospheric propagation of VLF/ULF radio waves, in [35], the pre-, co-, and post-seismic effects are discussed in connection with the $M > 5.5$ earthquakes that took place in the South-Eastern Mediterranean in September–October 2021 and in January 2022. In a review of seismogenic VLF/ULF wave phenomena [36], it is stressed that during the last three decades considerable progress has been made in the investigation of electromagnetic effects connected with earthquakes and in earthquake forecasting.

Presently, the possible generation mechanism of ionospheric anomalies before an earthquake is widely discussed in scientific literature [37–39], where the connection between the lithosphere and ionosphere during the time of earthquake preparation is treated through the concept of Global Electric Circuit (GEC). In our former publication [11], we traced the process of successive transfer of seismogenic disturbances from the lithosphere up to ionosphere height before the M = 4.2–6.0 earthquakes. The data presented in this study can be considered a direct experimental confirmation of the propagation of seismogenic disturbance from the lithosphere up to the ionosphere. In agreement with the concept of lithospheric–atmospheric–ionospheric coupling, it is supposed that the role of an initiating link between the lithosphere and ionosphere involves the ionization of the near-surface atmosphere.

In the present article, the monitoring results of the Doppler frequency shift signal are considered, which was measured on a more than 3000 km long two-hop radio path prior to and in the time of the 6 February 2023 Turkey earthquake. The ionospheric response is discussed here using an analysis of the ionograms obtained by the ionosondes in Nicosia (Cyprus) and El Arenosillo (Spain), which were operating in the mode of vertical ionosphere sounding.

2. Material and Methods

2.1. The Doppler Sounding Technique

An effective method to control the state of the ionosphere above the sources of earthquakes is registration of the Doppler frequency shift of a short-wave radio signal reflected from the ionosphere. This method is based on the Doppler effect, which appears with the variation in electron concentration in the ionosphere. Continuous monitoring of the Doppler frequency shift of the reflected radio signal is carried out at the experimental base of the Institute of Ionosphere in Almaty (Kazakhstan). The results of these measurements are applied, in particular, in the search for anomalous effects during the preparation period and in the time of earthquakes.

The hardware–software complex of Doppler measurements used for this purpose is based on the phase-locked frequency loop (PLL) operation principle [40]. Using PLL permits measurement of the Doppler shift of a larger amplitude beam in conditions of multipath radio wave propagation. The PLL converts the Doppler frequency to the proportional voltage at the output of a phase detector. The width of the hold-off band of the PLL loop is 15 Hz and the non-linearity of its frequency conversion characteristic is below 0.46%. Such parameters are quite sufficient for a high-quality measurement of the Doppler frequency shift of ionospheric signal. The measurement accuracy of Doppler frequency is 0.01 Hz or better, which is 1.5–2 orders below the level of background frequency variation in the F-region of the ionosphere. The receiver of the Doppler radiosonde is stabilized by a rubidium frequency standard.

As a source of sounding radio signal, the transmitters of broadcasting radio stations are used. The ionosonde can operate in the frequency range of (1–30) MHz; selection of

the most appropriate frequency for the day- and night-time is made according to the BBC Frequencies and Sites Catalog [41]. The frequencies are switched automatically by a special computer program, accounting for the time of day and season of the year. After digitization of the signal gained in the output of the PLL phase detector, the data are stored as files in the memory of a personal computer. Time synchronization of the control computer is made via Internet from an NTP-server of an atomic frequency and time standard. The highly automated operation mode of the equipment ensures whole-day measurement of the Doppler frequency shift of ionospheric signal.

In the time of the *M*7.8 Turkey earthquake, monitoring of the Doppler shift variation was made at an inclined two-hop radio path "Kuwait—Institute of Ionosphere (Almaty)", with a length of 3010 km. The disposition of the path relative to the epicenter of the earthquake is shown in Figure 1. In this scheme, the red ellipses indicate the projection onto the Earth of the points of radio wave reflection in the ionosphere (sub-ionospheric points). As it is seen there, in the case of the Turkey earthquake, the first sub-ionospheric point falls inside the Dobrovolsky circle, the radius of which depends on the magnitude ($R_D = 10^{0.43 \cdot M}$ km) and determines the size of the zone of deformation processes that existed in the lithosphere during the period of earthquake preparation [42]. For the *M*7.8 earthquake, $R_D = 2259$ km, while the distance from the epicenter to the first sub-ionospheric point equals 1591 km (see Section 3.1.1 below). In Figure 1, it can be seen how large the area encompassed by the processes of earthquake preparation is.

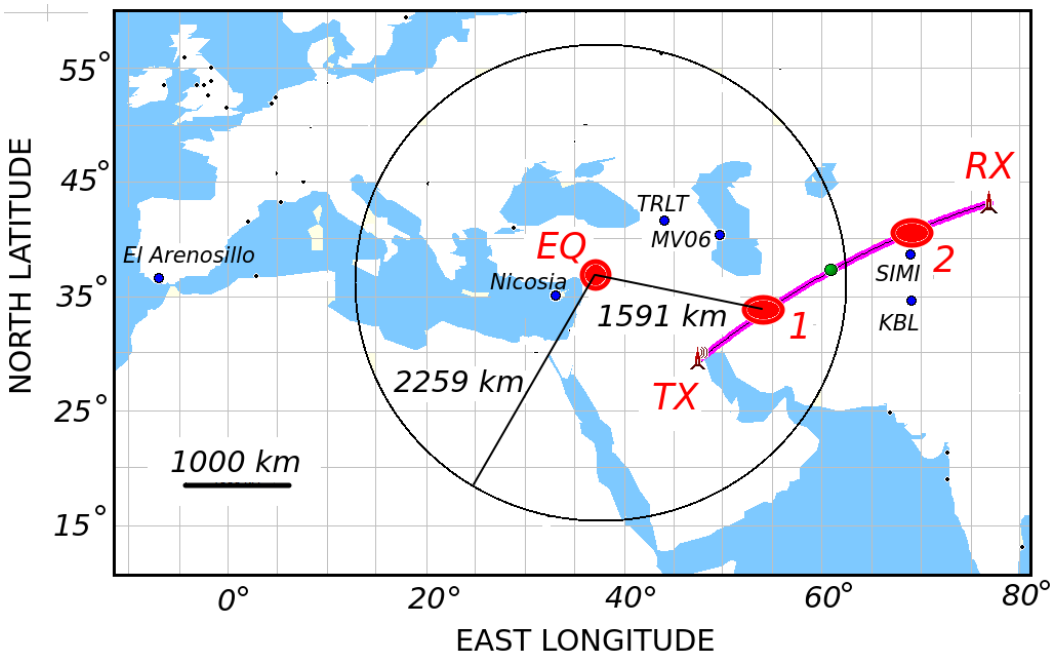

Figure 1. Disposition scheme of the radio path "Kuwait—Institute of Ionosphere (Almaty)" relative to the epicenter of the 6 February 2023 *M*7.8 earthquake in Turkey. *EQ*—earthquake epicenter, *TX*—transmitter, and *RX*—receiver of the Doppler ionosonde; red ellipses 1 and 2 indicate the sub-ionospheric points of the first and second hops of the sounding radio wave. The circumference indicates the size of the Dobrovolsky radius R_D. The seismological and ionosonde stations mentioned in the text are marked with blue circles.

2.2. Geomagnetic Conditions

Further on in this article, the anomalous effects detected in the ionosphere both before and after the 6 February 2023 Turkey earthquake will be considered. In principle, ionospheric disturbances can be due not only to seismic processes but also to enhanced geomagnetic activity. It is known that geomagnetic storms and sub-storms cause a strong disturbing effect on the ionosphere [8]. Even during weak storms with a Kp index below 5, and under geomagnetic disturbances with $Kp = 4$, the ionosphere may be in a dis-

turbed state [43]. Seemingly, the mentioned Kp values are a threshold below which the geomagnetic activity does not considerably influence the ionosphere. In one of the recent works [44], the values $Kp < 3$, $Dst > -30$ nT were assumed as a sign of relatively quiet geomagnetic conditions, at which it is possible to consider the potentially seismogenic anomalies in the ionosphere.

In our work, the data on geomagnetic activity in January–February 2023 were taken from the site of the World Data Center for Geomagnetism in Kyoto [45]. The distributions of the ap, Dst, and Kp indices are shown in Figure 2. As it follows from these plots, the ap index was kept within the interval of (10–18) nT, the Dst index was slightly varying between -8 and -23 nT, and the three-hour geomagnetic index Kp did not exceed an average value of 3. Only on 18 and 21 January did the Kp index rise up to 4. For these reasons, we can conclude that for the time from 17 January until the earthquake date on 6 February, the geomagnetic conditions remained relatively quiet.

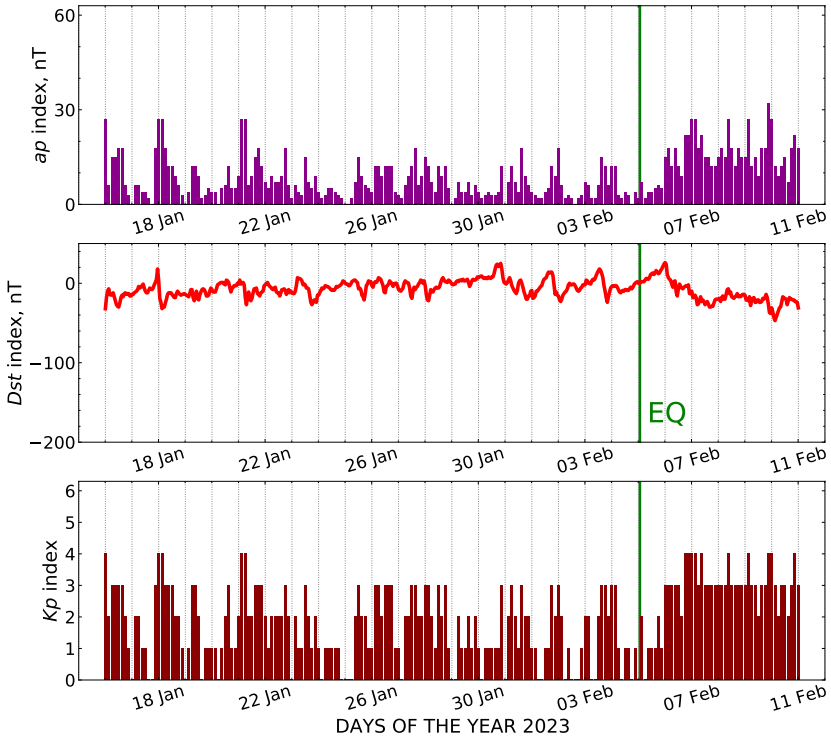

Figure 2. Variation of geomagnetic indices in January—February 2023 according to the data [45]. The bold vertical line in the plots marks the main shock of the 6 February 2023 earthquake (EQ) in Turkey; the dotted lines correspond to the beginning of each date.

3. Ionospheric Effects of the Earthquake

In Figure 3, a fragment of the variation record is presented of the Doppler frequency shift that was received on 6 February 2023 after propagation of the sounding radio signal over the two-hop radio path "Kuwait—Institute of Ionosphere (Almaty)". The original measurement data are shown in the plot with a thin line; the bold line indicates the same data after their smoothing by a 10-point running average filter. It is seen that at the moment of 01:34:12 UTC, ~17 min (988 s) after the main shock of the Turkey $M7.8$ earthquake, the Doppler ionosonde registered a disturbance in the ionosphere. The disturbance lasted about 160 s, and its double amplitude, more than 2 Hz, was essentially above the level of background fluctuations.

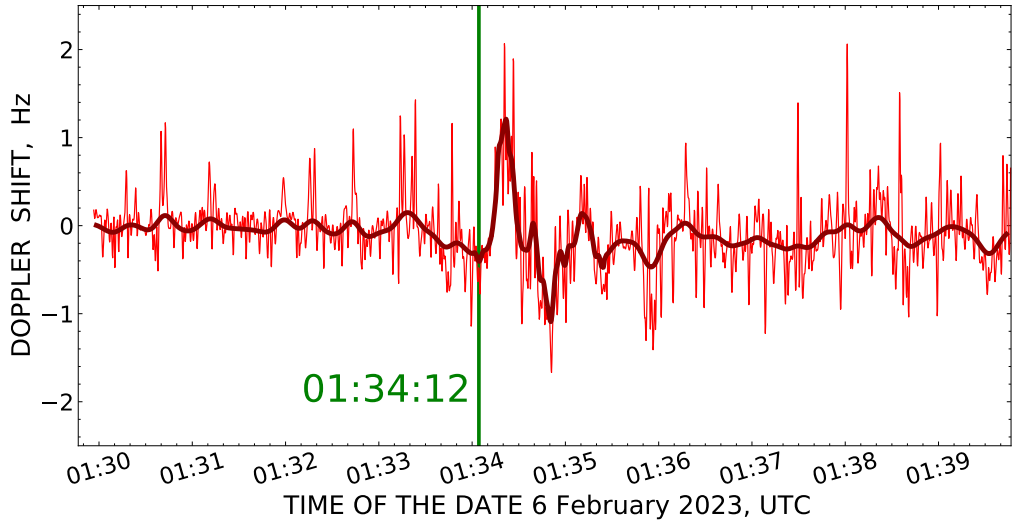

Figure 3. The response in the Doppler frequency shift of ionospheric signal to the *M*7.8 earthquake in Turkey on 6 February 2023, as detected at the radio path "Kuwait—Institute of Ionosphere (Almaty)". Thin curve—original measurements; bold curve—same data smoothed by a 10 points running average filter. The vertical line indicates the beginning of the ionosphere disturbance in the reflection point of radio waves at 01:34:12 UTC.

The subject of the next paragraphs is an investigation of the possible reasons for this interesting effect on the variation in the Doppler frequency shift and on its connection with the earthquake in Turkey.

3.1. Seismoacoustic Effect in the Ionosphere

3.1.1. Calculation of the Trajectory and Reflection Height of the Sounding Radio Wave

The geographical coordinates and the height of the points of radio wave reflection in the middle of the first and second hops of the radio path used was defined on the basis of the profile of electron concentration *Ne*, which, in turn, was calculated at site [46] using the IRI2016 model. The international etalon model of the ionosphere IRI2016, together with the set of coefficients IGRF13, permits the deduction of various parameters of the ionosphere for a specific combination of geographical location, date, and time.

For the first hop, the calculation of electron concentration was made for the time moment on 6 February 2023, 01:34:12 UTC, which corresponds to the appearance of the seismogenic disturbance in the record of the Doppler frequency shift signal (see Figure 3). For better accuracy, into the initial data of the IRI2016 model was inserted the actual index of solar activity for the previous day, $F10.7 = 144$, taken from site [47], as well as the value of critical frequency $f0F2 = 4.1$ MHz obtained from the ionogram of the NI135 ionosonde [48]. The ionosonde is situated on Cyprus island (N35.03°, E33.16°) at the close distance of 1928 km from the sub-ionospheric point of the first hop and at nearly the same latitude as this point (N33.951°, E54.709°). The closeness of latitudes suggests similarity of the ionosphere parameters in both points for one and the same *local* time. In the longitudinal direction, the ionosonde station is displaced by 20.84° relative to the sub-ionospheric point, which corresponds to 1.39 h in time units. Considering this time difference, the ionogram in site [48] was taken for the moment of 02:50:00 UTC. The ionogram and the estimated altitude profile of electron concentration are reproduced in Figure 4.

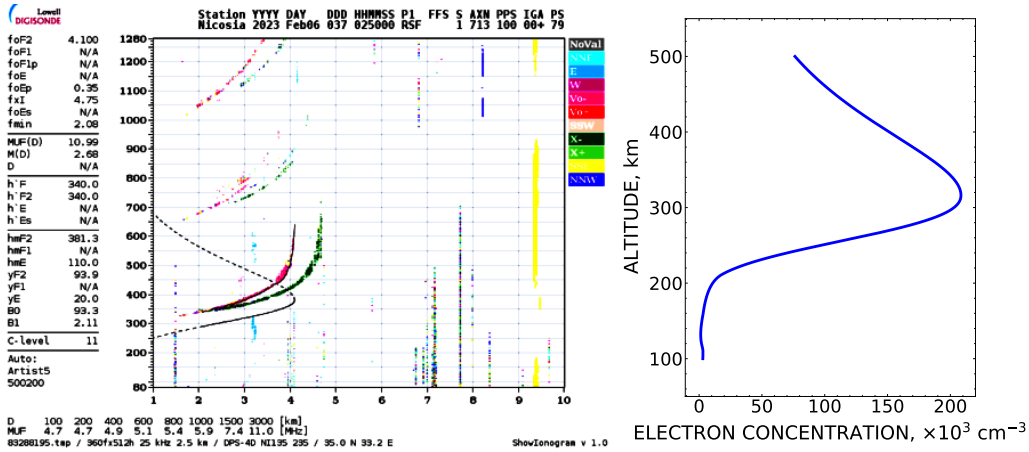

Figure 4. The ionogram of the NI135 ionosonde [48] and the corresponding altitude profile of electron concentration for the middle point of the first hop of the radio path of the sounding radio wave.

Using the profile of electron concentration, the trajectory of radio wave propagation was calculated by a special program from site [46], which took into account the geomagnetic field according to the IGRF13 model for the ordinary component. The parameters of the radio path obtained as a result of the calculation are as follows:

- The geographical coordinates of the sub-ionospheric point at the first hop of the radio path are N33.951°, E54.709°, with the corresponding distance between this point and the epicenter of the Turkey earthquake along the earth's surface being $D = 1591$ km;
- The height of radio wave reflection at the first hop of the radio path is $H = 232.49$ km;
- The distance of the radio wave reflection point in the ionosphere from the transmitter is 827.4 km;
- The distance between the transmitter and the point of radio wave reflection from the earth's surface is 1504.1 km;
- The azimuth of the radio path trajectory in the direction from the transmitter to the receiver is 51.74°, and the elevation angle of the trajectory at the point of the transmitter is 20.6°;
- The azimuth of the vector of the geomagnetic field in the reflection point is 4.89°, and the angle between this vector and the vertical Z axis is 52.85°.

The calculation method of the second hop of the radio path was analogous. The sub-ionospheric point of the second hop was at a distance of 2756 km from the epicenter, well outside the Dobrovolsky circle. The estimated height of radio wave reflection in the ionosphere was 212.0 km.

The schematic of the radio signal propagation trajectory over the radio path "Kuwait—Institute of Ionosphere (Almaty)" is presented in Figure 5.

3.1.2. Calculation of the Arrival Time of the Surface Seismic Wave to the Sub-Ionospheric Point

To check the connection of the disturbance revealed in the record of the Doppler frequency shift signal (see Figure 3) with the earthquake in Turkey, it is necessary to know the arrival time of the surface seismic wave to the sub-ionospheric point at the first hop of the sounding radio wave. However, in the vicinity of the sub-ionospheric point there is no seismological station, the data of which could be used for this purpose.

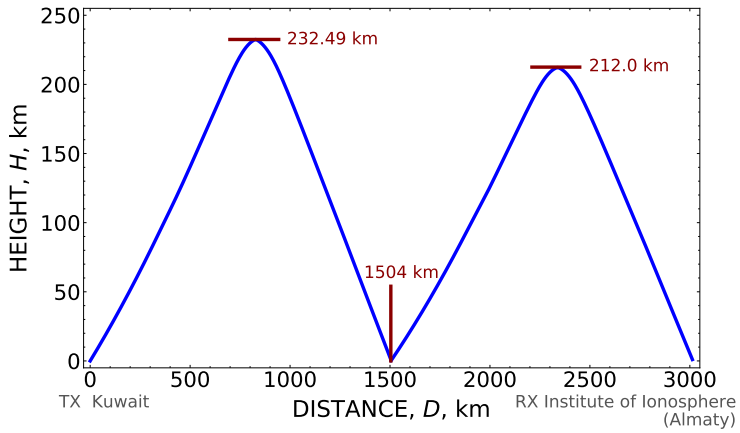

Figure 5. The trajectory of the two-hop radio path of Doppler measurements "Kuwait—Institute of Ionosphere (Almaty)".

Considering the direction and the distance from the epicenter of the earthquake to the sub-ionospheric point, the following seismological stations were selected for further analysis: TRLT in Trialeti, Georgia; MV06 in Guzdek, Azerbaijan; SIMI in Simiganj, Tajikistan; and KBL in Kabul, Afghanistan. The stations are listed in Table 1. The seismograms of the vertical Z-component of the speed of ground movement recorded at these stations were selected from the Internet site of the IRIS consortium [1] and reproduced in Figure 6. In accordance with the explanation given in [1] (https://ds.iris.edu/ds/support/faq/6/what-is-a-count-in-timeseries-data, accessed on 1 June 2023), *counts* designated along the *Y*-axis in the plot of Figure 6 are the codes of an analog-to-digital converter. The speed of the ground displacement expressed in units of m/s can be obtained by dividing *count* by a calibration number, which equals $3.27508 \cdot 10^9$ for the registration frequency of 0.02 Hz. On the plot, the *counts* of seismic data are additionally normalized into relative units for ease of viewing.

Table 1. Main parameters of the seismic waves registered at the seismological stations nearest to the epicenter.

Station	Coordinates	Epicenter Distance, km	V_p, km·s^{-1}	V_s, km·s^{-1}	V_p/V_s	V_R, km·s^{-1}	Propagation Time, t , s [1]
SIMI: Simiganj, Tajikistan	N38.66° E69.01°	2801	8.618	4.739	1.818	3.704	429.5
KBL: Kabul, Afghanistan	N34.54° E69.04°	2890	8.704	4.764	1.819	3.696	430.5
MV06: Guzdek, Azerbaijan	N40.37° E49.68°	1153	7.790	4.350	1.790	3.731	426.4
TRLT: Trialeti, Georgia	N41.57° E44.15°	785	7.696	4.289	1.794	3.504	454.1
sub-ionospheric reflection point	N33.54° E54.00°	1591	–	–	–	3.700 [2]	430.0

[1] Calculated as $t = 1591\,\text{km}/V_R$. [2] For the sub-ionospheric point, the value V_R was calculated as an average of the stations SIMI and KBL.

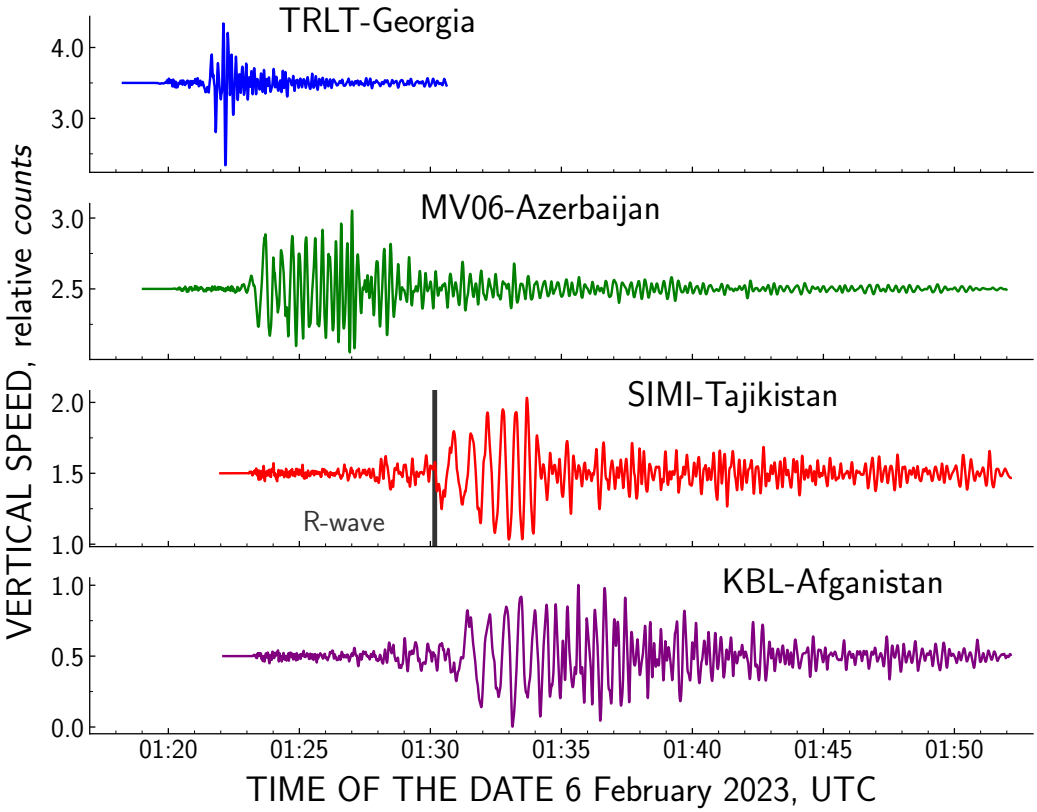

Figure 6. The fragments of the record of the vertical Z-component of the speed of ground movement measured on 6 February 2023 at various distances from the earthquake epicenter at the seismological stations TRLT, MV06, SIMI, and KBL. Scaling of the vertical axis is explained in Section 3.1.2.

Importantly, looking from the epicenter, the azimuth of the sub-ionospheric point was $A = 100^\circ$. This was the direction in which the surface Rayleigh wave was propagating from the epicenter after the earthquake. The azimuths, relative to the epicenter, of the nearest to the sub-ionospheric points of seismological stations TRLT and MV06 are 49° and 68°, respectively. The azimuths of the more distant stations—SIMI, 77°, and KBL, 86°—are closer to the direction $A = 100^\circ$. This is why the stations SIMI and KBL were chosen for determination of the arrival moment of the surface seismic wave to the sub-ionospheric point.

Among the data of the SIMI and KBL stations, two types of seismic waves can be distinctly selected: the arrival of the volumetric waves (P and S) and that of the surface Rayleigh wave. By each seismogram, the propagation velocity of the P and S waves, V_P and V_S; the relation V_P/V_S; and the velocity of the Rayleigh wave, V_R, were calculated. These values are also listed in Table 1.

The time necessary for a seismogenic disturbance to reach the sub-ionospheric point at the first hop of the sounding radio wave was estimated as $t = 1591\ \text{km}/V_R$. It was at the arrival moment of the surface Rayleigh wave to the sub-ionospheric point that the acoustic waves were capable of propagating in a vertical direction up to the ionosphere height by the law of infrasonic waves [49] and being registered by the Doppler ionosonde.

As it follows from the data presented in Table 1, at time $t_1 = 430\,\text{s}$, the surface Rayleigh wave had reached the sub-ionospheric point, which was situated at a distance of 1591 km from the epicenter. The time delay between the beginning of the ionospheric disturbance in Figure 3 and the moment of the Turkey earthquake was 998 s. Then, the acoustic wave, which had arisen in the sub-ionospheric point and was moving in a vertical direction, reached the reflection point of the sounding radio wave in the ionosphere after $\Delta t = 998\,\text{s} - 430\,\text{s} = 568\,\text{s}$. Step-by-step propagation of the seismogenic disturbance up to the ionosphere height is illustrated by the scheme in Figure 7.

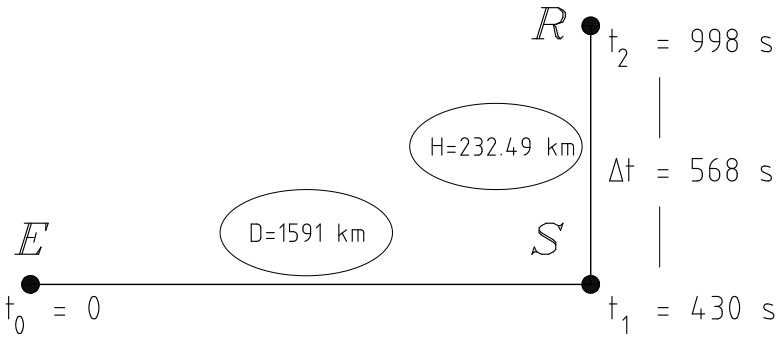

Figure 7. The time diagram of the seismogenic disturbance propagation from the earthquake epicenter up to the reflection point of the sounding radio wave in the ionosphere: *E*—epicenter, *R*—reflection point, and *S*—its projection onto the surface of the Earth. Estimation of the height *H* and distance *D* to the sub-ionospheric point is discussed in Section 3.1.1.

3.1.3. The Propagation Time of Infrasonic Wave Up to the Reflection Point of the Sounding Radio Wave

Based on the experimental data and calculation of the trajectory of radio wave propagation, in previous paragraphs it was defined that the infrasonic formed by the surface seismic wave reached the point of radio wave reflection at the height of 232.49 km after 568 s. Presently, these data will be compared with an estimation of the height that an acoustic wave could reach in 568 s deduced from the altitude profile of the sound speed. The calculation method, based on the international atmosphere model NRLMSISE-00, is described in [49,50].

In Figure 8, the results of the calculation of the profile of sound speed and of the time delays of an acoustic wave's arrival to different heights in the ionosphere are presented. The calculation was made for the geographical coordinates of the sub-ionospheric point at the first hop of the radio path "Kuwait—Institute of Ionosphere (Almaty)" during the time of the Turkey earthquake and for the index of solar activity $F10.7 = 144$ given for the previous day at site [47].

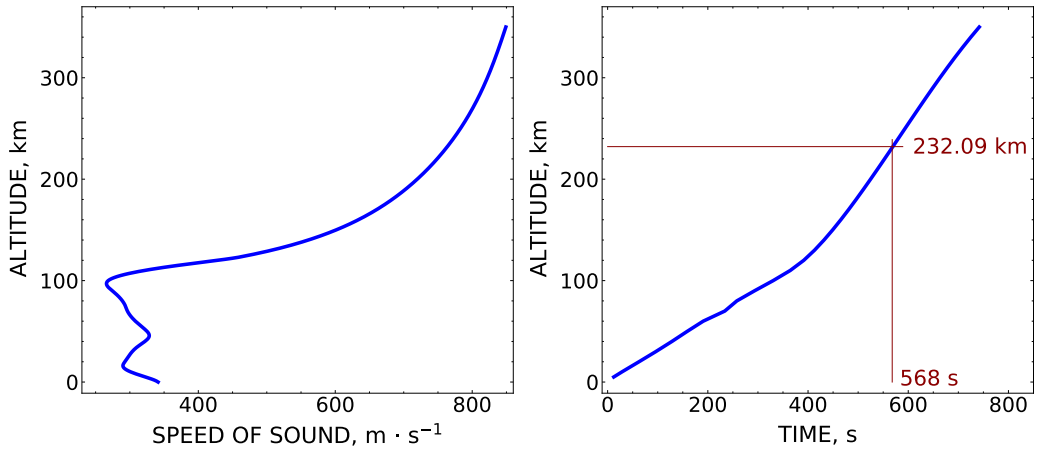

Figure 8. The estimated altitude profile of the sound speed (left), and the arrival moment of an acoustic wave at different heights in the ionosphere by the *M*7.8 Turkey earthquake.

As it follows from the right plot of Figure 8, in 568 s the acoustic wave should reach the altitude of 232.09 km in the ionosphere; according to the previous calculation of the trajectory of the sounding radio wave, the height of the reflection point was 232.49 km. Thus, the evaluation of the reflection height of radio waves made by the two independent methods

showed a very good coincidence between the experimental and calculation data, with only a negligible difference between the resulting estimations (232.49 − 232.09 = 0.4 km).

3.1.4. Comparison of the Doppler Frequency Shift Variation with the Seismic Waveform

In Figure 9, the waveform of the seismic wave propagating from the epicenter of the 6 February 2023 Turkey earthquake, as detected at KBL seismological station (Kabul, Afghanistan), is compared against the variation record of the Doppler frequency shift. For convenience, the data series presented here are normalized accordingly to the maxima of their amplitudes and the seismogram is displaced along the time axis to superimpose with the beginning of the disturbance in the ionosphere. The Doppler shift data shown in Figure 9 are smoothed by a 10-point running average filter.

It is seen in Figure 9 that both the variation in the Doppler frequency shift and the surface seismic Rayleigh wave have similar periods, which lie within the limits of (38–44) s. The best coincidence between the waveforms is observed for the two leading periods, which is confirmed by calculation of the correlation coefficients r presented in Table 2 and in Figure 10. Such close correlation of the two leading wave packets confirms that the disturbances observed in the ionosphere were initiated by the passage of the Rayleigh wave and supports the conclusion of the acoustic origin of the detected ionospheric response.

It should be noted that by observation of co-seismic disturbances at a *weakly*inclined radio path, close to the vertical sounding of the ionosphere, the correlation coefficients between the ionospheric and seismic data series had larger values of $r > 0.90$ and r∼0.98 for two wave packets [12,51]. These observations were confirmed by the model calculation in [52].

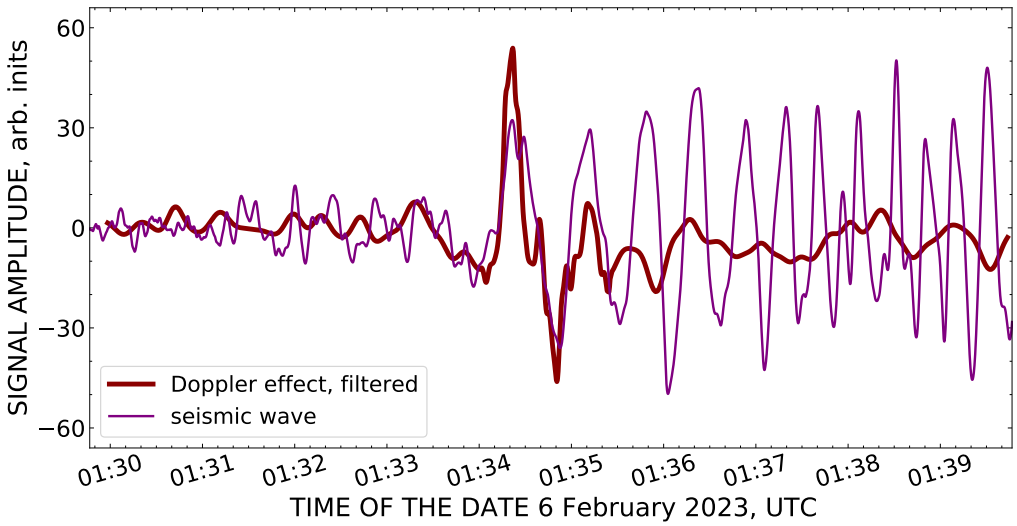

Figure 9. The record of the Doppler shift of ionospheric signal, after smoothing by the 10-point running average filter, in comparison with the seismogram taken at the KBL seismological station.

Table 2. The correlation coefficients between the waveforms of the signal of Doppler frequency shift and the surface seismic Rayleigh wave.

	Correlation Coefficients, *r*, in Dependence on the Number of Wave Periods (1–4) Participating in Comparison of Waveforms			
Seismological Station	**1**	**2**	**3**	**4**
KBL: Kabul, Afghanistan	0.859	0.785	0.611	0.546
SIMI: Simiganj, Tajikistan	0.855	0.742	0.497	0.456

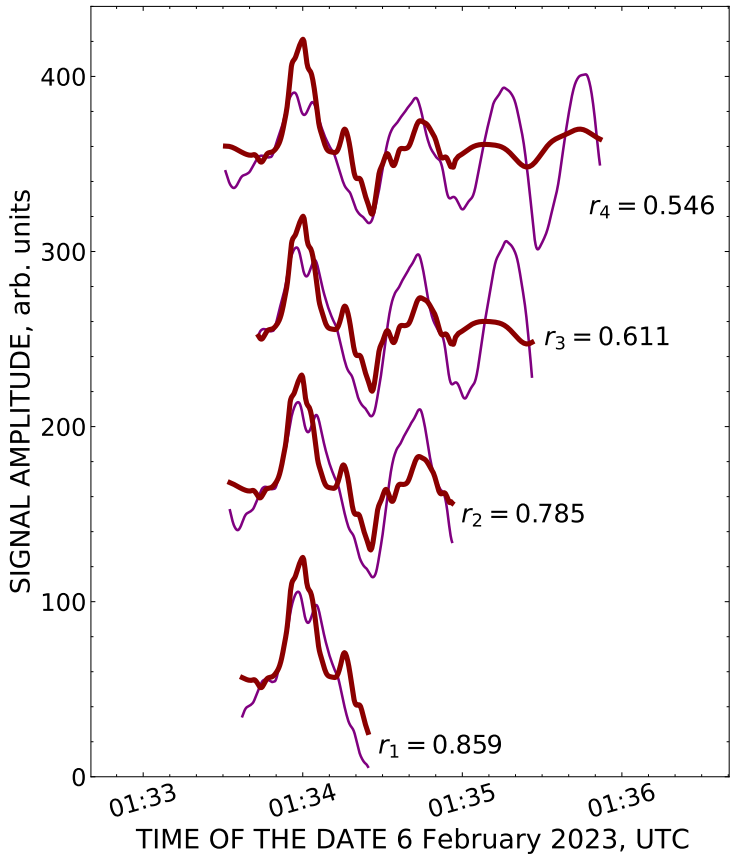

Figure 10. The change in correlation coefficient values depending on the number of compared waveform periods of the Doppler frequency shift record and of the surface seismic wave. Thick line—the fragment of the record of the Doppler frequency shift; thin line—the fragment of the Z-component seismogram made at the seismological station KBL.

As seen in Figure 10, by increasing the number of compared periods, the value of the correlation coefficient decreases. Indeed, the acoustic waves generated by a surface seismic wave influence vast regions in the ionosphere. Any exact coincidence in the shapes of all wave packets of the Doppler shift signal should not be expected since the radio track is inclined and the sounding radio wave, when reflected, travels a fairly long way in the ionosphere. An absence of any correlation ($r < 0.25$) was estimated also for the TRLT (Trialeti, Georgia) and MV06 (Guzdek, Azerbaijan) seismological stations.

As a summary of the presented data, it can be stated that the catastrophic 6 February 2023 earthquake in Turkey induced noticeable co-seismic ionospheric effects, which were caused by the vertical movement of the Earth during the passage of the surface Rayleigh wave. Even at a distance of 1591 km from the epicenter, the effect of the earthquake was detected by the Doppler ionosonde that was operating on an inclined two-hop radio path with a total length of more than 3000 km.

3.2. Pre-Seismic Ionospheric Effects

3.2.1. The Variation in the Critical Frequency $f0F2$

Studying the ionosphere variability before an earthquake is important both for revealing the precursors of large earthquakes and for understanding the connection between the appearance of anomalous effects in the ionosphere with the processes of earthquake preparation in the lithosphere. In the present paragraph, an analysis is made on the appearance of pre-seismic ionospheric disturbances in the variation in the critical frequency $f0F2$ during the period of 1 December 2022 to 2 April 2023.

The values of the critical frequency $f0F2$ with a 5 min registration interval were taken from the digital ionogram database (DIDBase) of the Global Ionosphere Radio Observatory [48]. The data of the ionosondes NI135 (Nicosia, Cyprus; N35.03°, E33.16°; 422 km from the epicenter of the 6 February 2023 Turkey earthquake) and EA036 (El Arenosillo, Spain; N37.10°, W6.70°; 3887 km epicenter distance) were used for the purpose. For the analysis, the initial 5 min $f0F2$ frequency data were averaged each day; next, a running average filter was applied to the resulting daily values, with averaging over 10 data points (days) and with backward shifting to one point. The result of this procedure is presented in the top-left plot of Figure 11.

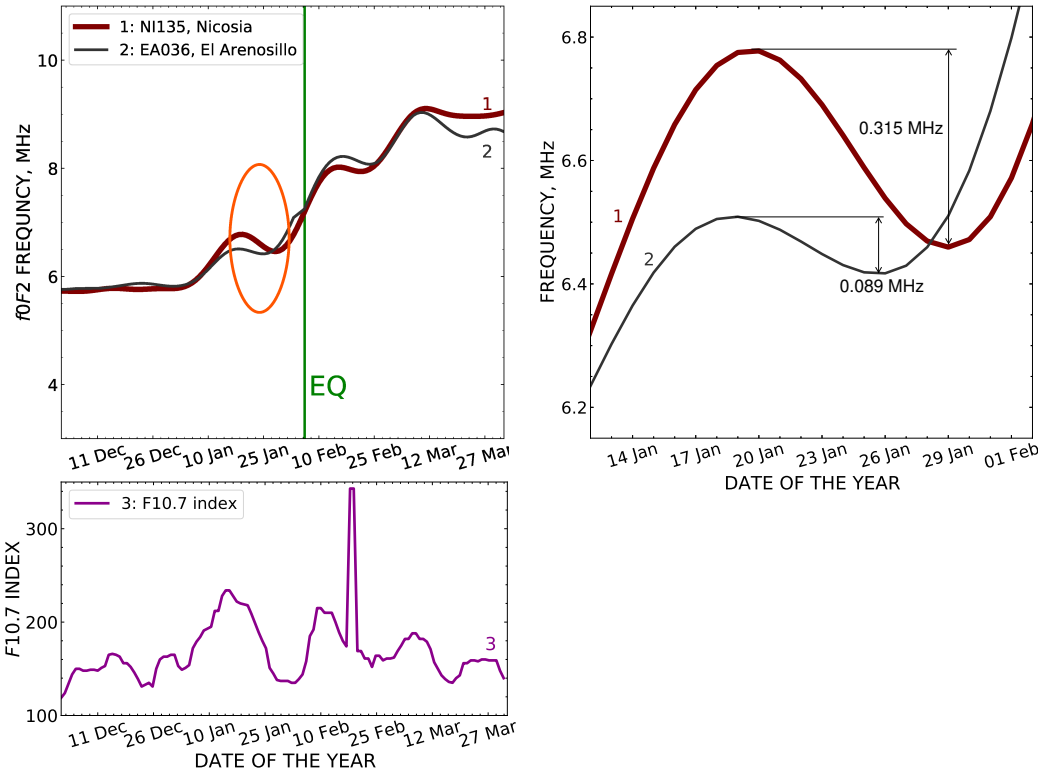

Figure 11. Comparison of the variation in critical frequency $f0F2$ according to the ionosonde data of NI135 (1) and EA036 (2), as well as the solar activity index $F10.7$ (3) measured from 1 December 2022 to 2 April 2023. The moment of the 6 February 2023 Turkey earthquake (EQ) is marked by a vertical line. The time period of 10 January until 3 February is highlighted by an ellipse in the left frame and shown enlarged in the right frame.

During the time preceding the 6 February 2023 Turkey earthquake, an unusual change in the critical frequency $f0F2$ was detected in the NI135 ionogram compared with the data of the more distant EA036 ionosonde; in the top left frame of Figure 11, this effect is distinguished by an ellipse. As seen in the plot, approximately 8 days before the earthquake, a noticeable drop occurred in the values of critical frequency registered by the two ionosonde stations at different distances from the epicenter, which reached its minimum on 29 January.

It should be stressed that during the considered period, the geomagnetic environment remained quiet and geomagnetic storms were absent from 17 January to 14 February. This follows from the variation in the $F10.7$ index taken at site [47] and shown in the bottom plot of Figure 11.

It is known also that a few days prior to the earthquake, a rise in solar activity took place, which might influence the variation in $f0F2$. In such a case, it is natural to expect that the response of the ionosphere would be the same in both ionospheric stations, NI135 and EA036, which are hosted at nearly the same latitude. Nevertheless, such a similarity was not observed: as it follows from the right top plot of Figure 11, the amplitude of the critical frequency variation at the NI135 station was 3.5 times higher than at the EA036

point. It is also important that, relative to the earthquake epicenter, the station NI135 is situated at a distance of ∼420 km, within the limits of the Dobrovolsky circle, while the El Arenosillo one is at a much larger distance of ∼3880 km and outside the earthquake preparation zone defined by the Dobrovolsky radius.

Thus, the said anomalous effect in the $f0F2$ variation was the only one that happened during the whole observable time interval before the $M7.8$ Turkey earthquake and under quiet geomagnetic conditions. This permits the theory that the drop in the critical frequency $f0F2$ with a minimum on 29 January, 8 days before the main shock, may be an ionospheric disturbance caused by the preparation process of the earthquake.

It is interesting also that among the $f0F2$ variation in the plot of Figure 11, a quasi-periodicity can be traced, comparable with the variation in the $F10.7$ index, which reflects the 27-day rotation period of the Sun. At the same time, after the earthquake, in the interval between 22 and 24 February 2023, at the NI135 station, no noticeable change of the critical frequency was detected, even at with the abrupt rise of the $F10.7$ index on 17–20 February 2023.

3.2.2. The Doppler Frequency Shift of Ionospheric Signal

For the search of ionospheric precursors of the 6 February 2023 Turkey earthquake, an analysis of the Doppler frequency shift variation in ionospheric signal measured before the earthquake at the inclined, 3010 km long, two-hop radio path "Kuwait—Institute of Ionosphere (Almaty)" was conducted. As mentioned above (see Section 3.1.1), the sub-ionospheric point of the first hop on this path was situated at a distance of 1591 km from the epicenter, inside the Dobrovolsky circle. The Doppler ionosonde of the Institute of Ionosphere has been constantly operating for many years, and every evening from 18h UTC until the morning of the next day at 6h UTC it has used the radio path "Kuwait—Institute of Ionosphere (Almaty)" at the frequency of 5860 kHz. Presently, an analysis of these data is made for the period 17 January–23 February 2023 using the mean daily values of the Doppler frequency shift. In Figure 12, the daily means are plotted by the bold solid curve; the thin curve indicates the same values after application of the running average filter over four points.

As seen in Figure 12, on 29 January, 8 days prior to the main shock, an increase in the Doppler frequency appeared followed by its abrupt rise, which started 3 days before the earthquake and was continuing during the time of aftershock activity. To estimate the statistical significance of this effect, the background record of the Doppler frequency made between 17–29 January, i.e., before the beginning of any anomalous disturbances, was compared against the time series of Doppler data measured since 29 January until the date of the Turkey earthquake on 6 February. For comparison, the mean values and standard deviations were defined for the two data sets; then, based on the calculated Student criterion $t = 5.61$, the confidence level of the difference between the data was obtained, $p < 0.001$. Consequently, the background data series and the data acquired in the period of the earthquake preparation significantly differ.

Thus, emergence of the disturbances in the ionosphere 8 days before the earthquake was registered by the two independent methods, the Doppler and ionogram, which enhances the importance of the revealed effect.

The remarkable coincidence in time should be noted, approximately 8 days before the earthquake, between the appearance of pre-seismic anomalous effects among the variations of both the Doppler frequency shift of ionospheric signal and the critical frequency $f0F2$ (see Section 3.2.1). This coincidence was observed within the limits of Dobrovolsky radius, i.e., inside the region of deformation processes in the lithosphere, which existed due to earthquake preparation. An appearance of seismo-ionospheric disturbances 7–8 days prior to major earthquakes was reported in [53]. It is also interesting to note that during a similar time interval, 3–10 days before the main shock, preparation of an $M_w7.2$ earthquake was detected by a multi-parametric investigation of the atmosphere [54].

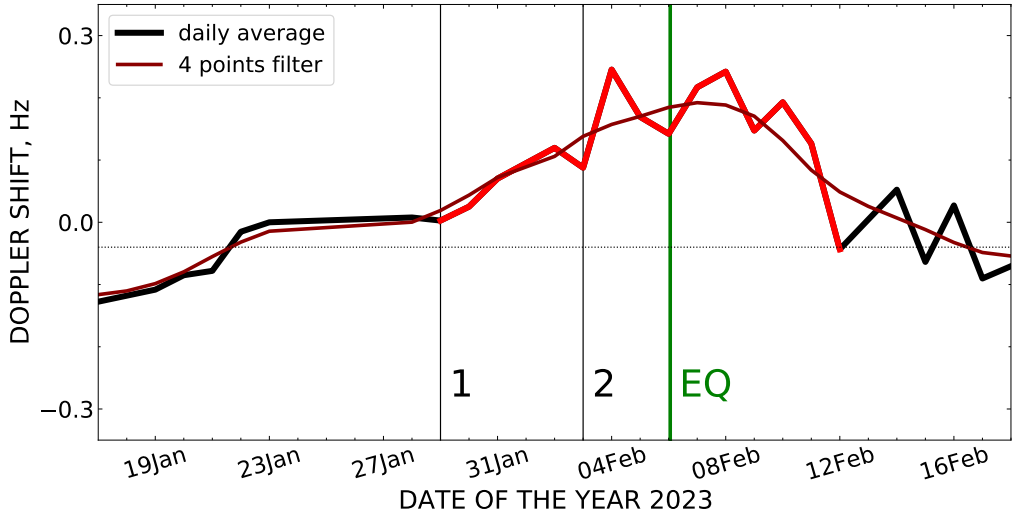

Figure 12. Mean daily values of the Doppler frequency shift of ionospheric signal registered at the "Kuwait—Institute of Ionosphere (Almaty)" radio path in January–February 2023. Thick curve—average of the Doppler shift values measured during a day; thin curve—same data after smoothing by a 4-point running average filter. The thick vertical line indicates the moment of the 6 February 2023 Turkey earthquake (EQ); lines 1 and 2 mark two preceding rises of the Doppler frequency on 29 January and 3 February. The mean value of undisturbed Doppler frequency in the period between 17 and 29 January is indicated by the horizontal dotted line.

According to literature [24–28,55], although different methods were used for the detection of seismogenic disturbances, a response in the ionosphere generally arises 3–16 days before an earthquake. As for the possible generation mechanism of pre-seismic ionospheric disturbances, in [37–39], the process of radon exhalation is considered as one of the leading factors of ionization in the lower atmosphere. In turn, the conductivity change in the atmosphere because of the ionization results in the modification of the ionosphere through the medium of the atmospheric electric field. Such processes encompass a considerable volume in the ionosphere above the region of earthquake preparation.

Previously, realization of the mechanism of lithospheric–atmospheric–ionospheric coupling was demonstrated in our publication [11], where complex observations are presented on the variation in the gamma radiation background both under the soil and in the near-Earth atmosphere, with simultaneous registration of the disturbances in the F2 layer of the ionosphere by a Doppler ionosonde. In that experiment, the anomalies in the behavior of the radiation background and in the Doppler frequency shift of the ionospheric signal were detected 7 days before an *M*4.2 earthquake, the source of which was at the depth of 15 km and only 5 km distance from the measurement equipment. In the present work, one more step is made towards experimental confirmation of the concept of lithospheric–atmospheric–ionospheric coupling by consideration of the revealed ionospheric disturbances in connection with the processes that took place in the lithosphere during the preparation of the *M*7.8 earthquake in Turkey.

4. Conclusions

Prior to and during the time of the catastrophic *M*7.8 Turkey earthquake, anomalous effects were found in the variation in the Doppler frequency shift of ionospheric signal, which was measured on an inclined two-hop radio path "Kuwait—Institute of Ionosphere (Almaty)". The origin of these effects is connected with different propagation mechanisms of seismogenic disturbance up to the height of the ionosphere.

1. On 6 February 2023, at 01:34:12 UTC, ∼17 min (988 s) after the main shock, a coseismic disturbance was detected in the variation in the Doppler frequency shift of ionospheric signal. The total duration of the effect was 160 s and its double amplitude was above 2 Hz, which considerably exceeds the background fluctuation of Doppler

frequency. The effect observed on the variation in Doppler frequency was a result of penetration into the ionosphere of the acoustic waves, which were generated by the surface seismic Rayleigh wave. The sequence of the disturbance propagation includes the time necessary for the Rayleigh wave to cover the distance from the epicenter to the first sub-ionospheric point and the spreading time of acoustic waves from the surface of the Earth up to the reflection point of the sounding radio wave in the ionosphere.

2. A considerable correlation degree ($r = 0.859$) was revealed between the registered waveforms of the Doppler frequency shift and of the surface seismic Rayleigh wave. The correlation diminishes when increasing the number of compared waveform periods.
3. Evaluation, by the two independent methods, of the height reached by the acoustic waves in the ionosphere and of the reflection height of the sounding radio wave demonstrates a good coincidence between the experimental and calculated data, and gives close estimates that differ only by 0.4 km.
4. Above the preparation region of the earthquake, as defined by the Dobrovolsky radius, the anomalous effects were found in the ionosphere among the variations of the Doppler frequency and of the critical frequency $f0F2$. Thus, 8 days before the earthquake, the Doppler ionosonde registered a noticeable rise in Doppler frequency, which continued to grow until the main shock; a decrease in the critical frequency $f0F2$ was detected simultaneously by the ionogram of the ionospheric station NI135 at Cyprus island.
5. An appearance of pre-seismic ionospheric anomalies detected before the $M7.8$ earthquake in Turkey by the two independent methods may be considered in accordance with the concept of lithospheric–atmospheric–ionospheric coupling.

Author Contributions: Conceptualization, N.S.; methodology, N.S. and S.N.; software, N.S. and A.S.; formal analysis, N.S., G.P. and A.K.; data curation, N.S. and A.S.; writing—original draft preparation, N.S. and G.P.; writing—review and editing, N.S., G.P., N.S. and A.S.; project administration, S.N., V.R. and V.Z.; funding acquisition, N.S. and S.N. All authors have read and agreed to the published version of the manuscript.

Funding: This research was funded by the Science Committee of the Ministry of Science and Higher Education of the Republic of Kazakhstan, grant number AP09260262 "Monitoring and research of geosphere interactions in the lithosphere–atmosphere–ionosphere system in geodynamically active regions". This research is supported by the postdoctoral Fellowship provided by Al-Farabi Kazakh National University.

Data Availability Statement: The data presented in this study are available on request from the corresponding author.

Conflicts of Interest: The authors declare no conflict of interest.

References

1. SAGE—Seismological Facility for the Advancement of Geoscience. Available online: https://ds.iris.edu (accessed on 1 June 2023).
2. Davies, K.; Baker, D. Ionospheric effects observed around the time of the Alaskan earthquake of March 28, 1964. *J. Geophys. Res.* **1965**, *70*, 2251–2253. [CrossRef]
3. Watts, Y.M.; Davies, K. Rapid frequency analysis of fading radio signals. *J. Geophys. Res.* **1960**, *65*, 2295–2301. [CrossRef]
4. Leonard, R.S.; Barnes, R.A. Observation of ionospheric disturbances following the Alaskan earthquake. *J. Geophys. Res.* **1965**, *70*, 1250–1253. [CrossRef]
5. Blank, E. Observations in the upper atmosphere of infrasonic waves from natural or artificial sources–A summary. *Ann. Geophys.* **1985**, *3*, 673–687.
6. Artru, J.; Farges, T.; Lognonne, P. Acoustic waves generated from seismic surface waves: Propagation properties determined from Doppler sounding observations and normal-mode modelling. *J. Int.* **2004**, *158*, 1067–1077. [CrossRef]
7. Liu, Y.; Tsai, Y.B.; Chen, S.W.; Lee, C.P.; Chen, Y.C.; Yen, H.Y.; Chang, W.Y.; Liu, C. Giant ionospheric disturbances excited by the M9.3 Sumatra earthquake of 26 December 2004. *Geophys. Res. Lett.* **2004**, *33*, L02103. [CrossRef]
8. Astafyeva, E. Ionospheric detection of natural hazards. *Rev. Geophys.* **2019**, *57*, 1265–1288. [CrossRef]

9. Laštovička, J.; Base, J.; Hruska, F.; Chum, J.; Sindelarova, T.; Horalek, J.; Zednik, J.; Krasnov, V. Simultaneous infrasonic, seismic, magnetic, and ionospheric observations in an earthquake epicenter. *J. Atmos. Sol.-Terr. Phys.* **2010**, *72*, 1231–1240. [CrossRef]
10. Krasnov, V.M.; Drobzheva, Y.V.; Chum, J. Infrasonic waves in the ionosphere generated by a weak earthquake. *J. Atmos. Sol.-Terr. Phys.* **2011**, *73*, 1930–1939. [CrossRef]
11. Salikhov, N.; Shepetov, A.; Pak, G.; Nurakynov, S.; Ryabov, V.; Saduyev, N.; Sadykov, T.; Zhantayev, Z.; Zhukov, V. Monitoring of gamma radiation prior to earthquakes in a study of lithosphere-atmosphere-ionosphere coupling in Northern Tien Shan. *Atmosphere* **2022**, *13*, 1667,
12. Chum, J.; Hruska, F.; Zednik, J.; Laštovička, J. Ionospheric disturbances (infrasound waves) over the Czech Republic excited by the 2011 Tohoku earthquake. *J. Geophys. Res.* **2012**, *117*, A08319. [CrossRef]
13. Chum, J.; Liu, J.Y.; Laštovička, J.; Fišer, J.; Mošna, Z.; Baše, J.; Sun, Y.Y. Ionospheric signatures of the April 25, 2015 Nepal earthquake and the relative role of compression and advection for Doppler sounding of infrasound in the ionosphere. *Earth Planets Space* **2016**, *68*, 24. [CrossRef]
14. Drobzhev, V.I.; Krasnov, V.M.; Salikhov, N.M. Ionospheric disturbances accompanying earthquakes and explosions. *Radiophys. Quant. Electr.* **1978**, *21*, 1295–1296. [CrossRef]
15. Drobzhev, V.I.; Zheleznyakov, E.V.; Idrisov, I.K.; Kaliev, M.Z.; Kazakov, V.V.; Krasnov, V.M.; Pelenitsyn, G.M.; Savel'ev, V.L.; Salikhov, N.M.; Shingarkin, A.D. Ionospheric effects of the acoustic wave above the epicenter of an industrial explosion. *Radiophys. Quant. Electr.* **1987**, *30*, 1047–1051. [CrossRef]
16. Krasnov, V.M.; Drobzheva, Y.V.; Laštovička, J. Recent advances and difficulties of infrasonic wave investigation in the ionosphere. *Surv. Geophys.* **2006**, *27*, 169–209. [CrossRef]
17. Laštovička, J. Lower ionosphere response to external forcing: A brief review. *Adv. Space Res.* **2009**, *43*, 1–14. [CrossRef]
18. Chum, J.; Urbář, J.; Laštovička, J. Continuous Doppler sounding of the ionosphere during solar flares. *Earth Planets Space* **2018**, *70*, 198. [CrossRef]
19. Chum, J.; Liu, J.Y.; Podolska, K.; Šindelářová, T. Infrasound in the ionosphere from earthquakes and typhoons. *J. Atm. Sol.-Terr. Phys.* **2018**, *171*, 72–82. [CrossRef]
20. Pulinets, M.S.; Budnikov, P.A.; Pulinets, S.A. Global ionospheric response to intense variations of solar and geomagnetic activity according to the data of the GNSS global networks of navigation receivers. *Geomagn. Aeron.* **2023**, *63*, 175–185. [CrossRef]
21. Salikhov, N.M.; Pak, G.D. Ionospheric effects of solar flares and earthquake according to Doppler frequency shift on an inclined radio path. *Bull. Nat. Acad. Sci. Kazakhstan Repub.* **2020**, *331*, 108–115. [CrossRef]
22. Kikuchi, T.; Chum, J.; Tomizawa, I.; Hashimoto, K.K.; Hosokawa, K.; Ebihara, Y.; Supnithi, P. Penetration of the electric fields of the geomagnetic sudden commencement over the globe as observed with the HF Doppler sounders and magnetometers. *Earth Planets Space* **2021**, *73*, 10. [CrossRef]
23. Salikhov, N.; Shepetov, A.; Pak, G.; Saveliev, V.; Nurakynov, S.; Ryabov, V.; Zhukov, V. Disturbances of Doppler frequency shift of ionospheric signal and of telluric current caused by atmospheric waves from explosive eruption of Hunga Tonga volcano on January 15, 2022. *Atmosphere* **2023**, *14*, 245.
24. Oyama, K.I.; Devi, M.; Ryu, K.; Chen, C.H.; Liu, J.Y.; Liu, H.; Bankov, L.; Kodama, T. Modifications of the ionosphere prior to large earthquakes: Report from the Ionosphere Precursor Study Group. *Geosci. Lett.* **2016**, *3*, 6. [CrossRef]
25. Conti, L.; Picozza, P.; Sotgiu, A. A critical review of ground based observations of earthquake precursors. *Front. Earth Sci.* **2021**, *9*, 676766. [CrossRef]
26. Picozza, P.; Conti, L.; Sotgiu, A. Looking for earthquake precursors from space: A critical review. *Front. Earth Sci.* **2021**, *9*, 676775. [CrossRef]
27. Ouzounov, D.; Pulinets, S.; Davidenko, D.; Rozhnoi, A.; Solovieva, M.; Fedun, V.; Dwivedi, B.N.; Rybin, A.; Kafatos, M.; Taylor, P. Transient effects in atmosphere and ionosphere preceding the 2015 *M*7.8 and *M*7.3 Gorkha-Nepal earthquakes. *Front. Earth Sci.* **2021**, *9*, 757358. [CrossRef]
28. Dong, L.; Zhang, X.; Du, X. Analysis of ionospheric perturbations possibly related to Yangbi M_s6.4 and Maduo M_s7.4 earthquakes on 21 May 2021 in China using GPS TEC and GIM TEC data. *Atmosphere* **2022**, *13*, 1725. [CrossRef]
29. Chen, C.H.; Sun, Y.Y.; Xu, R.; Lin, K.; Wang, F.; Zhang, D.; Zhou, Y.; Gao, Y.; Zhang, X.; Yu, H.; et al. Resident waves in the ionosphere before the *M*6.1 Dali and *M*7.3 Qinghai earthquakes of 21–22 May 2021. *Earth Space Sci.* **2022**, *9*, e2021EA002159. [CrossRef]
30. Heki, K. Ionospheric electron enhancement preceding the 2011 Tohoku-Oki earthquake. *Geophys. Res. Lett.* **2011**, *38*, L17312. [CrossRef]
31. Heki, K.; Enomoto, Y. Preseismic ionospheric electron enhancements revisited. *J. Geophys. Res. Space Phys.* **2013**, *118*, 6618–6626. [CrossRef]
32. Liu, J.Y.; Chen, S.W.; Chen, Y.C.; Yen, H.Y.; Chang, C.P.; Chang, W.Y.; Tsai, L.C.; Chen, C.H.; Yang, W.H. Seismo-ionospheric precursors of the 26 December 2006 *M*7.0 Pingtung earthquake doublet. *Terr. Atmos. Ocean. Sci.* **2008**, *19*, 751–759. [CrossRef]
33. Hayakawa, M.; Molchanov, O.A.; Ondoh, T.; Kawai, E. The precursory signature effect of the Kobe earthquake on VLF subionospheric signals. *J. Commun. Res. Lab. Tokyo* **1996**, *43*, 169–180. [CrossRef]
34. Chakraborty, S.; Sasmal, S.; Basak, T.; Ghosh, S.; Palit, S.; Chakrabarti, S.K.; Ray, S. Numerical modeling of possible lower ionospheric anomalies associated with Nepal earthquake in May, 2015. *Adv. Space Res.* **2017**, *60*, 1787–1796. [CrossRef]

35. Politis, D.Z.; Potirakis, S.M.; Sasmal, S.; Malkotsis, F.; Dimakos, D.; Hayakawa, M. Possible pre-seismic indications prior to strong earthquakes that occurred in southeastern Mediterranean as observed simultaneously by three VLF/LF stations installed in Athens (Greece). *Atmosphere* **2023**, *14*, 673. [CrossRef]
36. Hayakawa, M.; Schekotov, A.; Izutsu, J.; Nickolaenko, A.P.; Hobara, Y. Seismogenic ULF/ELF wave phenomena: Recent advances and future perspectives. *Open J. Earthq. Res.* **2023**, *12*, 45–113. [CrossRef]
37. Pulinets, S.; Davidenko, D. Ionospheric precursors of earthquakes and Global Electric Circuit. *Adv. Space Res.* **2014**, *53*, 709–723. [CrossRef]
38. Pulinets, S.A.; Ouzounov, D.P.; Karelin, A.V.; Davidenko, D.V. Physical bases of the generation of short-term earthquake precursors: A complex model of ionization-induced geophysical processes in the lithosphere-atmosphere-ionosphere-magnetosphere system. *Geomagn. Aeron.* **2015**, *55*, 521–538. [CrossRef]
39. Parrot, M.; Tramutoli, V.; Liu, T.J.; Pulinets, S.; Ouzounov, D.; Genzano, N.; Lisi, M.; Hattori, K.; Namgaladze, A. Atmospheric and ionospheric coupling phenomena associated with large earthquakes. *Eur. Phys. J. Spec. Top.* **2021**, *230*, 197–225. [CrossRef]
40. Salikhov, N.M.; Somsikov, V.M. The program- and hardware complex for registration of the Doppler frequency shift of ionosphere radio-signal over earthquake epicenters (in Russian). *Bull. Nat. Acad. Sci. Kazakhstan Repub.* **2014**, *296*, 115–121.
41. BBC Frequencies and Sites. Available online: https://www.short-wave.info (accessed on 1 June 2023).
42. Dobrovolsky, I.P.; Zubkov, S.I.; Miachkin, V.I. Estimation of the size of earthquake preparation zones. *Pure Appl. Geophys.* **1979**, *117*, 1025–1044. [CrossRef]
43. Kurkin, V.I.; Polekh, N.M.; Zolotukhina, N.A. Effect of weak magnetic storms on the propagation of HF radio waves. *Geomagn. Aeron.* **2022**, *62*, 104–115. [CrossRef]
44. Liu, J.; Zhang, X.; Yang, X.; Yang, M.; Zhang, T.; Bao, Z.; Wu, W.; Qiu, G.; Yang, X.; Lu, Q. The Analysis of lithosphere-atmosphere-ionosphere coupling associated with the 2022 Luding Ms6.8 earthquake. *Remote Sens.* **2023**, *15*, 4042. [CrossRef]
45. World Data Center for Geomagnetism, Kyoto. Available online: https://wdc.kugi.kyoto-u.ac.jp (accessed on 1 June 2023).
46. Community Coordinated Modeling Center. Available online: https://ccmc.gsfc.nasa.gov (accessed on 1 June 2023).
47. Laboratory of X-ray Astronomy of the Sun. Available online: https://tesis.xras.ru/en/ (accessed on 1 June 2023).
48. Global Ionosphere Radio Observatory. Available online: https://giro.uml.edu/ (accessed on 1 June 2023).
49. Krasnov, V.M.; Drobzheva, Y.V. Nonlinear acoustics in the in homogeneous atmosphere within the limits of analytical solutions. In *The printeryKROM*; KROM: St. Petersburg, Russia, 2018; p. 172.
50. Krasnov, V.M.; Kuleshov, Y.V. Variation of infrasonic signal spectrum during wave propagation from Earth's surface to ionospheric altitudes. *Acoust. Phys.* **2014**, *60*, 19–28. [CrossRef]
51. Haralambous, H.; Guerra, M.; Chum, J.; Verhulst, T.G.W.; Barta, V.; David, A.; Cesaroni, C.; Galkin, I.; Marta, K.; Mielich, J.; et al. Multi-instrument observations of various ionospheric disturbances caused by the 6 February 2023 Turkey earthquake. In *ESS Open Archive*; 2023. Available online: https://essopenarchive.org/users/617934/articles/643145-multi-instrument-observations-of-various-ionospheric-disturbances-caused-by-the-6-february-2023-turkey-earthquake (accessed on 25 July 2023).
52. Krasnov, V.M.; Drobzheva, Y.V.; Chum, J. Far-field coseismic ionospheric disturbances of Tohoku earthquake. *J. Atmos. Sol.-Terr. Phys.* **2015**, *135*, 12–21. [CrossRef]
53. Sharma, K.; Dabas, R.S.; Sarkar, S.K.; Das, R.M.; Ravindran, S.; Gwal, A.K. Anomalous enhancement of ionospheric F2 layer critical frequency and total electron content over low latitudes before three recent major earthquakes in China. *J. Geophys. Res. Space Phys.* **2010**, *115*, A11313. [CrossRef]
54. Khan, M.M.; Ghaffar, B.; Shahzad, R.; Khan, M.R.; Shah, M.; Amin, A.H.; Eldin, S.M.; Naqvi, N.A.; Ali, R. Atmospheric anomalies associated with the 2021 M_w7.2 Haiti earthquake using machine learning from multiple satellites. *Sustainability* **2022**, *14*, 14782. [CrossRef]
55. Liu, J.Y.; Chen, Y.I.; Chuo, Y.J.; Chen, C.S. A statistical investigation of pre-earthquake ionospheric anomaly. *J. Geophys. Res.* **2006**, *111*, 5304. [CrossRef]